# NUMERICAL MODELING OF GEOFOAM EMBANKMENTS

by

Marie Perry Newman

A thesis submitted to the faculty of

The University of Utah

in partial fulfillment of the requirements for the degree of

Master of Science

Department of Civil Engineering

The University of Utah

December 2006

# ABSTRACT

In 2002, the Utah Department of Transportation (UDOT) completed the $1.4 billion I-15 Reconstruction Project in Salt Lake City, Utah. This project included the widespread use of geofoam embankments as light weight fill at important utility crossings and where proximity to existing buildings necessitated minimizing consolidation settlement. This paper presents construction and post-construction monitoring results of some of these embankments and numerical modeling of the field measurements. Fast Lagrangian Analysis of Continua (*FLAC)*, a finite difference program, was used to estimate the complex stress and strain behavior that develops in geofoam embankments. The authors used a bilinear elastic model to produce realistic and reliable estimations of the seating, gap closure and elastic compression of the geofoam embankment. Similar predictions are important for modeling and designing geofoam embankments and their connections to other systems. The estimation of the complex stress distribution that develops in a geofoam embankment has application to settlement, lateral earth pressure, slope stability and dynamic design of geofoam embankments.

This work is dedicated to my husband, Blake, and to my mother,

Kathrine Perry, for their unfailing support and encouragement.

TABLE OF CONTENTS

LIST OF FIGURES

# ACKNOWLEDGMENTS

I would like to thank Dr. Bartlett and Dr. Lawton for their help in the modeling and writing of this thesis. I also express appreciation to Clifton Farnsworth for his collection of the field data presented in this thesis. I especially wish to recognize the University of Utah College of Engineering for providing the Wayne Brown Fellowship for my graduate work and the Utah Department of Transportation for providing research funds.

# INTRODUCTION

In 1998 to 2001, the Utah Department of Transportation (UDOT) and a large construction consortium reconstructed I-15 in the Salt Lake Valley prior to the start of the 2002 Winter Olympic Games. Utah's rapidly growing population and traffic flow necessitated the widening of the freeway from six lanes to twelve lanes, but the awarding of the Winter Games gave momentum to the project and placed a rigid and challenging time constraint on its completion. In order to realize the reconstruction, UDOT chose to employ a design-build contracting mechanism, which resulted in a reconstruction that finished six months ahead of schedule and $32 million below the $1.4 billion reconstruction budget. During a 3.5-year construction period, 26 kilometers of urban interstate were reconstructed, which included 144 bridges and 160 mechanically stabilized earth (MSE) retaining walls. To achieve the accelerated construction, designers implemented relatively new geotechnical technologies including: lime cement column (LCC) supported embankment, accelerated drainage with prefabricated vertical drains (PVD), multi-staged construction embankment construction with geotextile reinforcement, 2-stage MSE walls, and light-weight embankment including scoria and geofoam embankments. This reconstruction project earned the ASCE 2002 Outstanding Civil Engineering Achievement Award. (Negussey et al. 2003)

The I-15 reconstruction alignment required the placement of large embankments (8 to 10 m high) atop soft clayey foundation soils. These soils had the potential to

produce primary consolidation settlement exceeding 1 meter at many locales. In some areas, pre-existing utility lines (e.g., high pressure gas lines, water mains, and communication cables) crossed beneath the freeway embankment and would be damaged by the settlement caused by new embankment construction. To allow these utilities to remain in-service without costly relocation and delays, the design team selected a lightweight embankment solution that would not produce damaging consolidation settlement. The design-build contractor, with UDOT's approval, chose to use expanded polystyrene (i.e., geofoam) embankment, which allowed the widening of the interstate without exceeding the preconsolidation stress of the underlying clayey soils; thus large and potentially damaging primary consolidation settlement was avoided. This extremely light-weight material, with a density of 18 kg / $m^3$, allowed rapid construction of full-height embankment in a short period of time without utility relocations. Approximately 107,000 cubic meters of geofoam currently resides underneath the newly reconstructed I-15 corridor in the Salt Lake Valley, making this project the single largest application of geofoam in the world to date. (Bartlett et al. 2001) Figure 1 shows the construction of a typical geofoam embankment at the I-15 reconstruction project.

During construction, UDOT Research personnel and researchers from the University of Utah and Syracuse University placed geotechnical instrumentation adjacent to and in the geofoam embankments at several locations. This paper discusses the field performance monitoring and numerical modeling of three geofoam placement locations: 3300 South Street exit ramp, State Street exit ramp and 100 South Street (Bartlett et al., 2001; Negussey et al., 2001; Negussey and Studlein, 2003). Geotechnical instrumentation was placed in order to measure the vertical and horizontal stresses that

Figure 1. Typical geofoam embankment construction on the I-15 Reconstruction Project in Salt Lake City, Utah.

develop in the geofoam embankment and underlying soils and to record the amount of settlement related to the static loading and long-term creep of the geofoam. Data from the fore mentioned arrays have been collected for approximately 5 years. This paper compares the field results from select arrays with numerical models that estimate the vertical and horizontal pressures distribution and vertical deformation that developed during the static loading of I-15 geofoam embankments. The modeling was performed using *FLAC* (Fast Lagrangian Analysis of Continua), which is a general finite difference program developed by Itasca (2005) for geomaterials. The model was calibrated with the field measurements and was used to develop a better understanding of the vertical and horizontal pressure distributions and vertical deformations that develop in this complex,

multi-layered system. Results of this study will improve the understanding and estimation of the stress distribution and strain behavior of geofoam embankments.

Strain in the geofoam array is a combination of seating, gap closure and elastic compression of the geofoam block. Reasonable estimation of this combination of strain is important to the performance of connections that exist between the geofoam embankment, the tilt-up panel wall, and the overlying pavement section. Also, the estimation of the complex stress distribution that develops in a geofoam embankment and the overlying system has application to settlement, lateral earth pressure, slope stability and dynamic design of geofoam embankments.

## TYPICAL GEOFOAM EMBANKMENT CONSTRUCTION

Because the I-15 reconstruction was predominately a widening of the existing interstate, a wedge-shaped geofoam embankment was typically constructed adjacent to and atop the pre-existing embankment. For our modeling, we generalized the typical construction cross-section for geofoam embankment to 5 layers. See Figure 2. Starting from the bottom, the first layer consisted of a minimum of 0.3 meters of base sand that was graded and leveled for the placement of the approximately 0.82-m high by 1.2-m wide by 4.9-m long geofoam blocks (uncut dimensions).

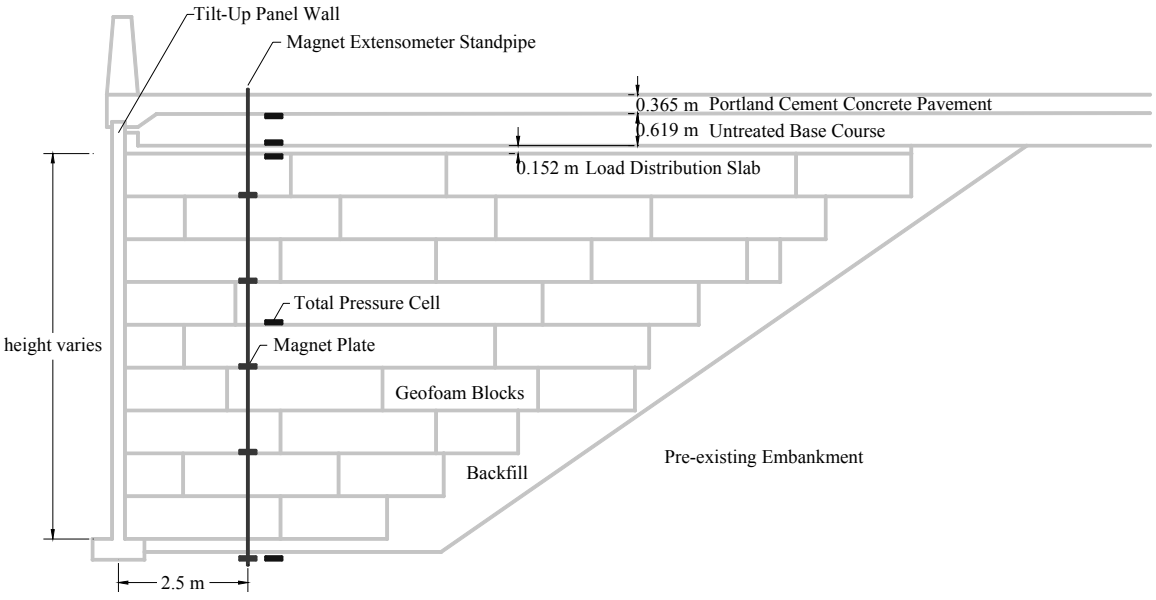


Figure 2. Typical cross-sectional view and instrumentation layout for the geofoam arrays at I-15, Salt Lake City, Utah.

Two materials made up the second layer: the pre-existing granular embankment, graded at a 1.5H:1V (33.7 degrees) backslope, and the adjacent geofoam, which abuts the existing embankment. Layer three consisted of a 0.150-meter thick reinforced concrete load distribution slab, used to protect the geofoam from local overstressing. Layer four was an untreated base course, about 0.610 meters thick, and layer five was an unreinforced portland cement concrete pavement, which was generally 0.356 meters thick.

After the placement of the geofoam embankment, a full-height tilt-up, prefabricated concrete panel wall was erected in a slotted strip footing. This wall permanently protects the face of the geofoam embankment from sunlight and petroleum spills. The panel wall was connected to the load distribution slab with a relatively rigid bar connection and a 0.1-meter gap was maintained between the vertical face of the geofoam embankment and the back side of the panel wall. The overlying concrete pavement slab was designed as a "moment" slab: it cantilevers over the top of the panel wall, but does not transfer any vertical load to the panel wall.

# INSTRUMENTATION

UDOT and the University of Utah have implemented an extensive, 10-year monitoring program of the construction and post-construction performance of the various geotechnologies used on the I-15 reconstruction (Bartlett and Farnsworth, 2004). In the geofoam arrays, magnet extensometers measured vertical compression of the geofoam embankment during placement of the overlying materials and pavement section. The magnet extensometer systems consist of base plates with annular magnets, PVC pipe, and a sensing probe. In this system, the plates move freely along the PVC pipe as the geofoam is compressed. To measure settlement, a probe is lowered through the pipe to measure the displacement of the plate magnets relative to the PVC riser pipe (Figure 2). Conductors within the probe locate the position of the plates and the reading device sounds when the magnet is located. (Negussey et al. 2003) A measuring tape attached to the probe makes it possible to read the position of the plate to the nearest millimeter.

Stainless steel vibrating wire (VW) total pressure cells rated at 170 kPa and 345 kPa measured the vertical and horizontal pressures that developed in the geofoam embankment. The VW pressure cells consist of two flat, circular disks, welded together with a liquid-filled cavity between the disks. The surrounding pressure compresses the liquid and the frequency of wire vibration correlates to pressure induced on the pressure cell as read by a sensor box.

## GEOFOAM ARRAYS

At the 3300 South Street off ramp, field performance data were collected at three arrays: the north array (station 25+371), middle array (station 25+347) and south array (station 25+315) (Bartlett et al. 2001). Because the middle and south arrays have the most comprehensive sets of data, we modeled these arrays. At the south array, there are nine layers of geofoam, generating a total geofoam height of about 7.4 meters. There are eight layers of geofoam at the middle array, producing a total geofoam height of about 6.6 meters.

Researchers installed magnet extensometer plates underneath the first geofoam layer in the base sand and at every other block layer interface. The plates were placed approximately 2.5 meters from the vertical face of the geofoam array. VW pressure cells at the 3300 South Street middle and south arrays were placed in four vertical positions at approximately 2.5 meters from the vertical geofoam face: 1) in the base sand at a depth of about 0.1 meters underneath the first layer of geofoam, 2) approximately in the middle of the geofoam mass, 3) directly above the load distribution slab in the untreated base course, and 4) just underneath the concrete pavement in the untreated base course (Figure 2). Where VW pressure cells rested on a geofoam block, hand-carved grooves accommodated the cylindrical pressure transducer. Also, a thin veneer of sand was placed around the edges of the pressure plate to reduce stress concentration. Figure 3

shows the 3300 South south array. Note the sand in the foreground, which conceals the pressure cell, and the PVC riser pipe in the background.

Additional VW pressure cells were deployed at the State Street off ramp. At this location, a full-height geofoam embankment abuts against a pile-supported bridge on the west end of the off ramp. Geofoam embankment supports the bridge approach slab and the adjacent pavement section. To the east, the off ramp and geofoam embankment diminish in height until the ramp reaches the grade of the adjacent State Street. See Figure 4. Along this off ramp, pressure cell measurements were collected at the bridge abutment (station 1+005), west array (station 1+118), middle array (station 1+131) and east array (station 1+158). At the bridge abutment, total pressure cells were oriented horizontally and vertically to measure the vertical and horizontal stresses that develop at the face of the concrete abutment and in the adjacent geofoam block. Three VW pressure cells were cast in the face of the concrete abutment to measure horizontal stresses. An additional two cells, one oriented vertically and the other oriented horizontally, were inserted in the adjacent geofoam block to measure the horizontal and vertical stresses, respectively. A precision cut was made in the geofoam block using a computerized hotwire cutter to obtain an exact fit for the VW pressure cell.

At the west array (bottom to top), there is a one-half height block layer, two full block layers and another one-half height block layer, resulting in a 2.46-meter total geofoam height. At the middle array, there are two layers of full height block of geofoam, making a 1.62-meter total geofoam height. At the east array, there is one full block layer of geofoam, generating a 0.82-meter total geofoam height. All pressure cells

Figure 3. Geofoam array at 3300 South south array, showing a concealed pressure cell, PVC riser pipe, and gaps between block layers.

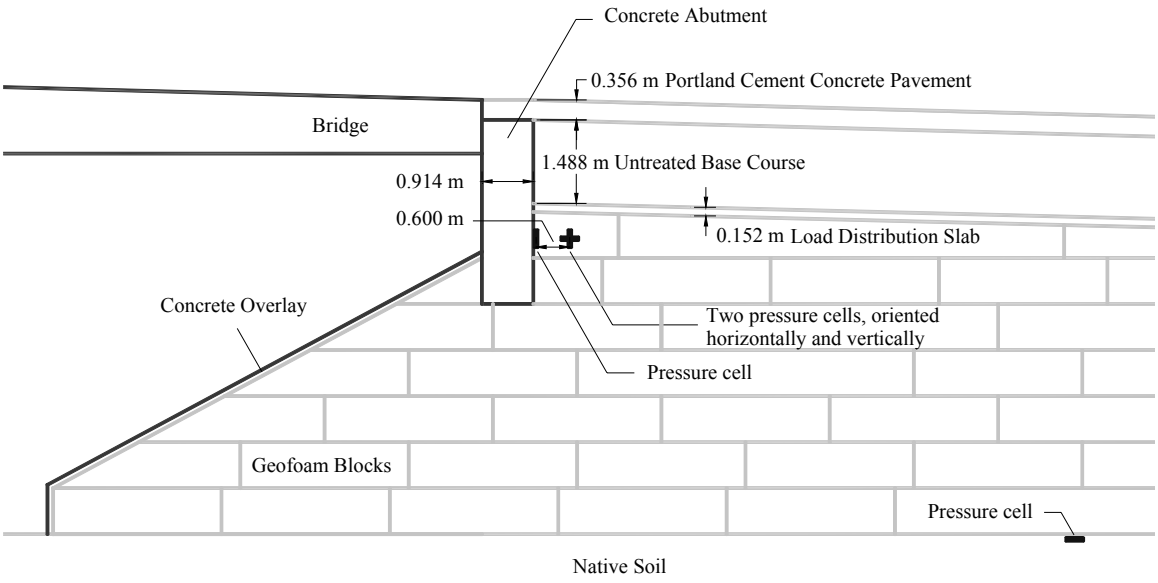


Figure 4. Geofoam cross-section (parallel to bridge) at the west end of the State Street off ramp.

for these three arrays were placed in the base sand, just below the lowest geofoam layer. No magnet extensometers were positioned in the geofoam at the State Street arrays.

At 100 South Street, near downtown Salt Lake City, UDOT and Syracuse University personnel installed instruments and collected data at two arrays: the north array (station 1+112) and the south array (station 1+123) (Negussey and Studlein, 2003). We chose to model the data from the south array. The geofoam block at the south array consisted of (from bottom to top) one-half height block layer, eight full height block layers and one-half height block layer, making the total height of the geofoam embankment about 7.3 meters. Magnet extensometer plates were installed underneath the first geofoam layer in the base sand and at every other block layer interface at approximately 2.5 meters from the vertical face of the geofoam array. Two pressure cells were embedded in the base sand at the south array. One cell was placed 1.473 meters from the face of the panel wall; the other was placed 2.692 meters from the face of the same wall. The latter cell malfunctioned and began recording negative pressures and will not be mentioned further.

## DATA INTERPRETATION

Many pressure cells located near the roadway surface showed a seasonal cycling of vertical pressure. This behavior is attributed to thermal expansion and contraction of the load distribution slab and/or portland cement concrete pavement and was most pronounced for pressure cells placed at the top or above the geofoam embankment (Bartlett et al., 2001). The cycling was not as visible in pressure cell data located in the middle of the geofoam mass or in the base sands. See **Figure 5**. We chose to compare the average of the summer or peak values with the *FLAC* results. Similarly, seasonal cycling was present in the magnet extensometer data. We chose to compare the average of the displacements measured by the magnet extensometers during the summer months with the *FLAC* results.

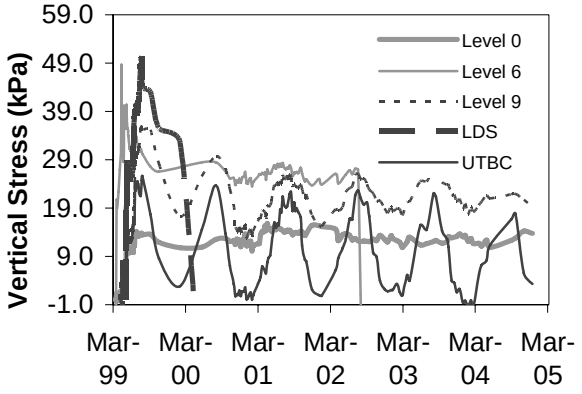


Figure 5. 3300 South Street south array cell data.

In a few cases, pressure cells located just above the load distribution slab recorded positive values for several months and then began to record negative values. If these cells recorded positive values for a few seasonal cycles, then the average value in the summer is plotted in subsequent stress figures. However, if data was only recorded for one cycle or less, the data for the cell was not used. This pressure cell behavior is probably due to malfunctioning of the cells, but it may also represent an actual unloading of the cell caused by creep settlement of the geofoam and interaction of the panel wall with the load distribution slab and overlying pavement section. Because the load distribution slab has a somewhat rigid connection with the tilt-up panel wall, any creep settlement of the geofoam could transfer unanticipated vertical loads to the wall and cause a subsequent unloading of the cells located just below the load distribution slab. Our models did not include this potential interaction. This issue requires further research and modeling.

## MATERIAL PROPERTIES

Material properties used in the *FLAC* modeling are given in Table 1. Type VIII geofoam, with a density of 18 kg/m$^3$ and a Poisson's ratio of 0.103, was used at all arrays (Bartlett et al., 2001; Benchmark 2003). Previous unconfined compression tests on 50-mm cube samples of Type VIII geofoam have produced unconfined compressive strengths between 97 and 111 kPa for five and ten percent axial strain, respectively (Bartlett et al. 2000). In the *FLAC* model, we used a cohesion value equal to 50 percent of the average compressive strength, approximately 50 kPa. Also, direct shear tests have been performed to measure the friction coefficients between sand and geofoam as well as between two layers of geofoam (Bartlett et al. 2000). Based on these tests, the friction angle between sand and geofoam is approximately 31° and friction angle between geofoam and geofoam is approximately 42° (Bartlett et al. 2000).

Table 1. Material properties for numerical models.

| Material | $\rho$ (kg/m$^3$) | $\nu$ | E (MPa) | K (MPa) | G (MPa) | $\varphi$ (°) | c (MPa) |
|---|---|---|---|---|---|---|---|
| Pre-existing soil<br>Base sand | 2160 | 0.350 | 100 | 111 | 37.0 | 35 | 0 |
| Geofoam $\sigma \leq 15$ kPa<br>Geofoam $\sigma > 15$ kPa | 18.00 | 0.103 | 1.70<br>10.0 | 0.714<br>4.20 | 0.771<br>4.53 | 35 | 0.025 |
| LDS<br>PCCP | 2400 | 0.180 | 30000 | 15600 | 12700 | 25 | 25 |
| UTBC | 2240 | 0.35 | 100 | 111 | 37.0 | 35 | 0 |

Values of Young's modulus for geofoam are a function of geofoam density; however, reported values in the literature can be somewhat variable due to sample size and edge effects. Researchers have measured moduli values of about 5 MPa from laboratory tests on small samples of Type VIII geofoam (Bartlett et al, 2000), but such tests may underestimate the true modulus of full-sized geofoam blocks due to crushing and damage of the edges of the samples. Recent testing on Type VIII full-size geofoam block has reported moduli values as high as 14 MPa (Elragi 2000). **Figure 6** shows the stress-strain relationship of a typical geofoam large-scale sample block.

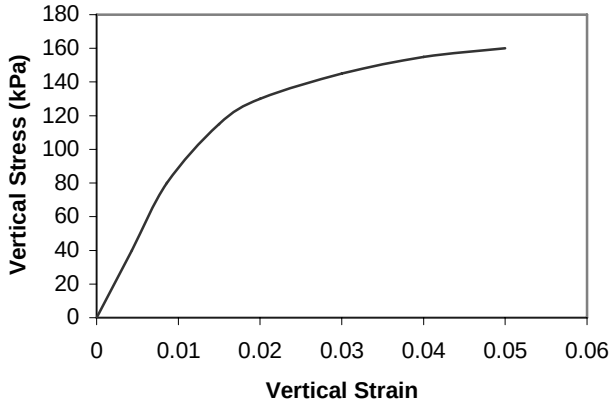


Figure 6. Typical laboratory stress-strain relationship of a large-scale geofoam block, adapted from Elragi (2000).

The estimation of Young's modulus becomes even more intricate because in addition to elastic compression of the geofoam, vertical strain resulting from gap closure of slightly curved block occurs upon initial loading of the geofoam embankment (Bartlett et al., 2000; Negussey and Studlein, 2003). Note the gaps between geofoam block layers at the 3300 South south array in Figure 3. Block curvature develops during block cooling and is most noticeable along the longest dimension of the block. Trimming the block can minimize or eliminate this curvature; however, the I-15 blocks, as manufactured, met the specified ± 0.5% dimensional and 5% flatness tolerances and trimming was not necessary by the project specifications. Still, block curvature was accounted for during the placement of the geofoam blocks. Laborers sighted down the long dimension of each block to determine the direction of curvature and placed the blocks concave down to achieve a tighter block fit. Nonetheless, complete seating and gap closure did not occur in the geofoam embankment until the final load, consisting of the combined weights of the load distribution slab, base materials and pavement section, had been placed atop the geofoam (Bartlett et al. 2001).

The curvature of the block and resulting gap closure upon loading produced extra complexity in our numerical modeling. To model this behavior, we used a bilinear elastic model. At low stress, a lower modulus value, $E_s$ represented seating and gap closure; at higher stress levels, a much higher modulus, E, represented the actual elastic compression of the geofoam embankment. To develop the parameters for the bilinear model, we used geofoam field performance data and analyses from the I-15 reconstruction at 100 South Street (Negussey et al. 2001). Negussey et al. (2001) plotted vertical stress and strain from field measurements and suggested a modulus of about 2.3 to 2.7 MPa to represent

seating and gap closure. In our models, we tested low stress moduli of 1.7, 2.3, and 2.7 MPa. In addition, we used a modulus of 10 MPa to represent the true elastic compression of the geofoam, which is an average value consistent with recent large block laboratory tests (Elragi, 2000). This higher modulus was used in the bilinear model whenever the calculated vertical stress at a point in the geofoam model exceeded 15 kPa. This break point was also developed based on plots of the field performance data from the 100 South Street geofoam array (Negussey et al. 2001). Figure 7 presents the results of Negussey et al. and compares the stress-strain curves from the north and south arrays at 100 South with the stress-strain curve presented in Figure 6 and with a typical bilinear modulus used in our modeling.

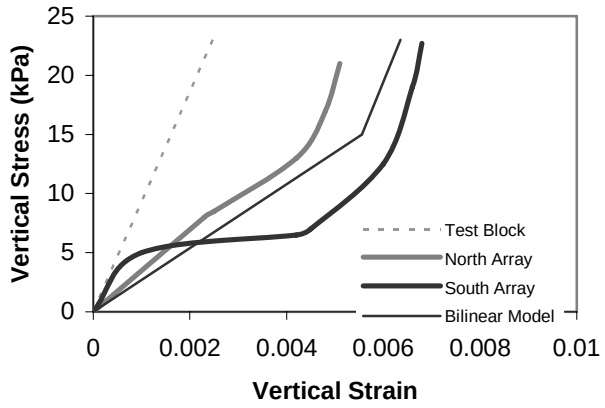


Figure 7. Stress-strain relationships from field data at 100 South, north and south arrays, from laboratory test data, and from the bilinear modulus used in modeling. Adapted from Negussey et al. (2001) and Elragi (2000).

Average properties represented the other materials in the numerical model. Properties for the load distribution slab and portland cement concrete pavement were estimated from average concrete properties (Itasca 2005 Structural Elements). See Table 1 for the properties used for base sand, pre-existing embankment, geofoam, load distribution slab (LDS), untreated base course (UTBC), and portland cement concrete pavement (PCCP). The table includes mass density ($\rho$), Poisson's ratio ($\nu$), Young's modulus (E), shear modulus (K), bulk modulus (G), friction angle ($\varphi$), and cohesion (c). It should be noted that only the seating modulus of 1.7 MPa is listed in Table 1 for geofoam, but the modeling considered and compared three low stress moduli (1.7, 2.3 and 2.7 MPa).

# MODELING APPROACH

In order to replicate the stages of construction of the geofoam embankment, the cross-sections were built incrementally in *FLAC*, starting from the bottom. First, the particular geometry for the entire embankment was inputted using construction cross-section drawings at the array locations. Then, the portland cement concrete, untreated base course, load distribution slab, geofoam and backfill layers were given null properties in the *FLAC* model and the model time-stepped until the unbalanced forces approached zero. This step modeled the placement of and the resulting stresses and compression in the base sand due to its self-weight. Following this, material properties were assigned to the geofoam and adjacent backfill region. *FLAC* time-stepped until it reached equilibrium. This represented placement of and resulting stresses and compression in the geofoam and backfill due to their self-weights. This step also produced additional displacement in the base sand from the placement of the geofoam and backfill. This additional displacement was added to the base sand displacements from the previous step. The stresses produced in this step resulted from the weights of the geofoam, backfill and base sand. Similarly, each subsequent layer was incrementally added to the model and the model was time-stepped until static equilibrium occurred. In the final step, all five layers existed in the model with non-null properties.

To create numerical stability, we fixed the side boundaries of the *FLAC* models in the "x" direction and fixed the bottom of the models in the "y" direction. Interfaces were

used to join the geofoam to the surrounding soil so as to allow the geofoam and soil to slide against each other. Otherwise, *FLAC* would have attached the soil and geofoam and the two materials would have moved together. In actuality, the two materials can settle independently and the use of interface nodes more realistically simulated the actual conditions.

In order to implement the bilinear elastic model, we wrote additional code in the *FLAC* command language, *FISH*, to check the vertical stress at one point in the geofoam mass and to then assign the appropriate modulus. If the vertical stress exceeded 15 kPa, the modulus changed from a relatively low value (e.g., 1.7-2.7 MPa) to a higher value of 10 MPa. As mentioned previously, the lower modulus, $E_s$, simulates the combined effects of seating and gap closure and the higher value of 10 MPa represents the true elastic modulus, E, of the geofoam mass.

To verify the *FLAC* modeling approach, we compared *FLAC* results with a finite element program, *SIGMA/W*, using a simple 3-layer system (Krahn 2004). For this comparison, the *FLAC* model was built incrementally, as previously described. The vertical stresses and elastic compression predicted by *SIGMA/W* and *FLAC* were compared at various points within the two models. The results agreed within 10% for both vertical stress and displacement for the simple 3-layer system; however, we noted that differences in results were larger when the complete geometry of the geofoam and adjacent granular embankment was modeled. Nevertheless, this latter comparison did not produce results that were sufficiently different so as to warrant further investigation and the differences were attributed to variations in the numerical approaches. In short, finite difference and finite element methods yield similar results. We chose the finite

difference approach because our future research entails modeling the potential sliding of geofoam embankment under seismic conditions and *FLAC* is well suited for these types of analyses.

# RESULTS

We used *FLAC* to analyze the stress-strain behavior of the geofoam embankments at 3300 South, State, and 100 South Streets using the bilinear elastic model. Our modeling process involved the comparison and calibration of the vertical stress distribution and differential displacements predicted by the *FLAC* model with those measured by the VW pressure cells and magnet extensometers at the various arrays.

Because of uncertainty in $E_s$, we analyzed and plotted *FLAC* results for low stress moduli of 1.7, 2.3, and 2.7 MPa and compared them against the measured results. We noted that the differential displacements between layers, presented in the plots hereafter, were measured shortly after the final dead loads (i.e., load distribution slab, untreated base and pavement) were placed; thus, the plotted displacement data do not include any creep settlement.

We found that variations in $E_s$ did not significantly change predictions of the vertical stress distribution; thus the vertical stress predictions are valid for $E_s$ values between 1.7 to 2.7 MPa. This is simply because the final state of stress in the geofoam embankment is generally greater than 15 kPa; hence the *FLAC* model used the higher modulus to calculate the final state of stress. However, variation of $E_s$ values does affect the differential displacement predictions, because a significant amount of the displacement occurs at stress levels below 15 kPa.

## 3300 South Street Off Ramp Arrays

Figure 8 and Figure 9 show the predicted results and measured data for the 3300 South Street south array at a distance of 2.5 meters from the vertical geofoam face. As shown in Figure 8, an $E_s$ value of 1.7 MPa yielded the best prediction of measured differential displacements. This graph also shows that the *FLAC* model predicts relatively uniform differential settlement (i.e., uniform strain) throughout the height of the geofoam, which is expected for a linear elastic material. However, the *FLAC* model somewhat under predicts the measured differential displacement between levels 6 and 8 and slightly over predicts the measured values between levels 8 and 9. The reason for the under prediction between levels 6 and 8 is unclear; however, the smaller measured and predicted differential displacements between levels eight and nine is due to the decrease in thickness of the geofoam block (i.e., one block as opposed to two). The under prediction betweens levels 6 and 8 and the over prediction between levels 8 and 9 are shown in every case of $E_s$ we analyzed.

Figure 9 presents a comparison of the predicted and measured vertical stresses at the 3300 South Street south array. In general, the *FLAC* model predicts a relatively uniform vertical stress of about 25 kPa in the geofoam embankment (levels 6 and 9) and about 13 kPa in UTBC layer just below the concrete pavement. The measured data are relatively similar at these elevations. However, the pressure cell placed just above the load distribution slab (LDS) shows considerably higher predicted pressure than what was measured. This pressure cell measured positive vertical stresses only for a few months and then began to record only negative values. It appears that this cell may have failed or

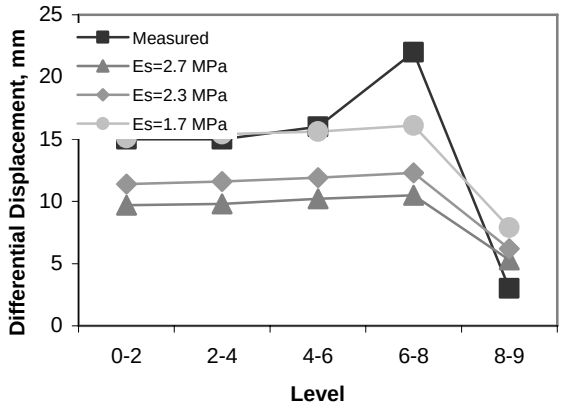


Figure 8. Predicted and measured differential displacements between geofoam layers for the 3300 South Street south array.

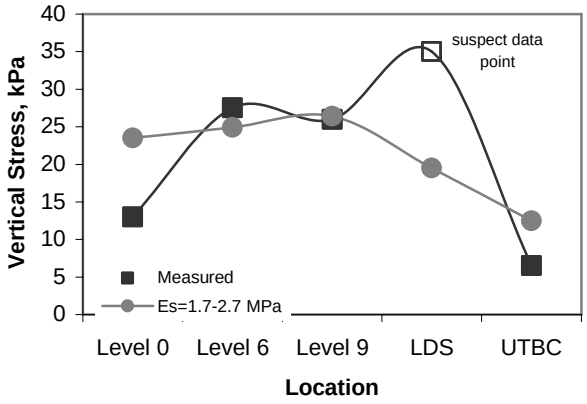


Figure 9. Predicted and measured vertical stresses for the 3300 South Street south array.

has in some way lost contact with the overlying road base. In either case, we believe that data from this cell should be disregarded.

*FLAC* over predicts the measured pressure in the base sand (level 0) by about 100% (Figure 9). We noted that there was a consistent trend in most of the *FLAC* models to over estimate the measured vertical stress in the base sand. Accounting for reasonable variations in the inputted modulus in the base sand did not greatly affect this over prediction. Elragi (2000), who also performed *FLAC* modeling of I-15 field data, obtained similar over predictions. He hypothesized that the base sand and geofoam had lost contact in an unexplained way. This led us to the conclusion that perhaps some other phenomenon, not accounted for in the *FLAC* model, affected the measurement of vertical stress in the base sand. For example, it is possible that curvature in the geofoam block is not allowing a uniform distribution of vertical stress in the underlying sand or some other type of partial arch is being developed.

Figure 10 shows the predicted and measured displacements at the 3300 South middle array. This array is similar to the south array, except the geofoam embankment at this location is only 8 blocks high. As before, the *FLAC* model predicted relatively uniform differential settlement throughout the geofoam embankment. However, the field measurements are more variable. Some of the variation may be due to errors in reading the magnet extensometers, block and/or construction irregularities, such as curved block, or other complex interactions in the geofoam. It is difficult to judge which $E_s$ value best matches the field measurements for this array, but perhaps 2.3 MPa is a reasonable estimate of the average behavior.

Figure 11 shows the measured and predicted vertical stresses at the 3300 South Street middle array. The *FLAC* model predicts rather uniform stress of about 25 to 30 kPa in the geofoam (levels 5 and 8) and somewhat lesser values just above the LDS and just below the pavement in the UTBC. As previously discussed, the measured stress base sand (level 0) is over predicted by the *FLAC* model. In addition, an unusually high stress of about 45 kPa was measured at level 5 by the pressure cell (**Figure 11**). Perhaps this may be attributed to a stress concentration caused by curvature or irregularities in the geofoam block shape.

State Street Off Ramp Arrays

Figure 12 and Figure 13 present pressures measured at the State Street off ramp arrays. (No magnet extensometers were installed at this location.) Figure 12 shows the horizontal and vertical stress measured at and near the abutment face (Figure 4). The first data points, labeled "abutment horizontal", represent the measured and predicted horizontal stresses corresponding to the pressure cell that was cast flush with the concrete abutment face to measure horizontal stress. The points labeled "geofoam horizontal" and "geofoam vertical" represent the measured and predicted horizontal and vertical stresses, from a vertically and a horizontally oriented pressure cell, respectively, inserted in the adjacent geofoam block (Figure 4). All three cells were installed at the same elevation. Figure 12 shows that the *FLAC* model reasonably estimates the measured pressures at and near the bridge abutment.

Figure 13 shows the predicted and measured vertical stress in the base sand at the west, middle and south arrays. As previously discussed, the stresses measured in the base sand were significantly over predicted by the *FLAC* model at these locations.

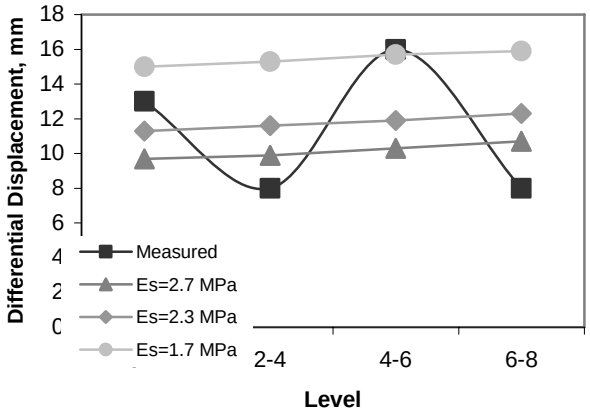


Figure 10. Predicted and measured differential displacements between geofoam layers for the 3300 South Street middle array.

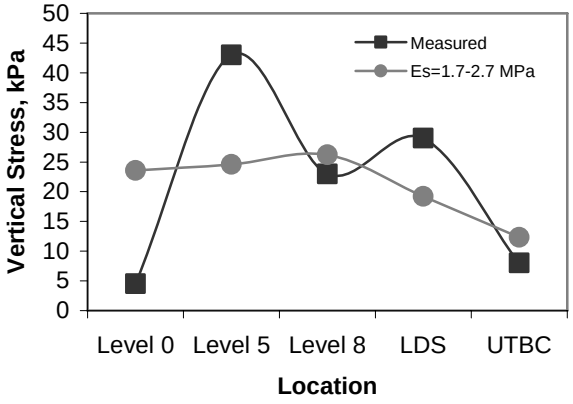


Figure 11. Predicted and measured vertical stresses for the 3300 South Street middle array.

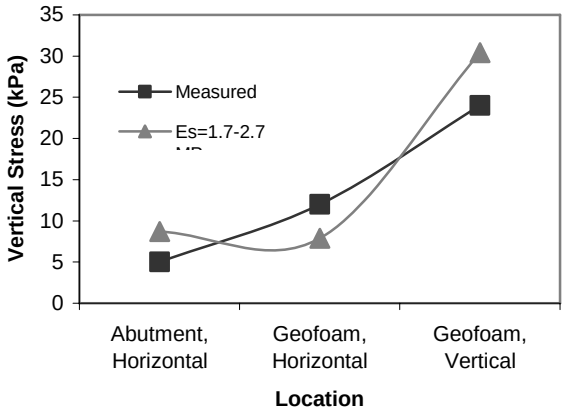


Figure 12. Predicted and measured horizontal and vertical stresses at and adjacent to the abutment at the State Street exit ramp.

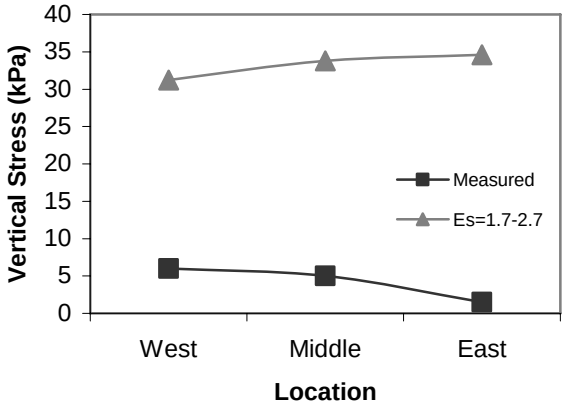


Figure 13. Predicted and measured vertical stresses in the base sand for the State Street exit ramp.

100 South Street Arrays

Figure 14 shows the predicted and measured differential settlement at 100 South Street, south array. The *FLAC* model predicts relatively uniform differential displacement throughout the geofoam embankment. Note that in this figure, the geofoam thickness for the last two data points is less than the first three points. The data and *FLAC* estimates for levels 7.5-8.5 are for only one layer of geofoam block, as opposed to two; the data and *FLAC* measurements for levels 8.5-9 are for a half block layer. Although the measured differential displacements for the south array are somewhat variable, the *FLAC* model does reasonably predict the differential displacement pattern. In addition, an $E_s$ value between 1.7 and 2.3 MPa appears to provide reasonable match to the field measurements.

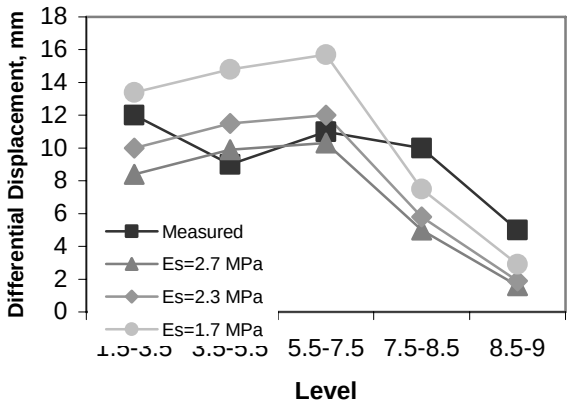


Figure 14. Predicted and measured differential displacements between geofoam layers for the 100 South Street south array.

The pressure cell data for the 100 South Street arrays are not plotted because only one pressure cell provided useable data. This pressure cell was placed in the base sand and measured a vertical stress of about 33 kPa; the *FLAC* model predicted a vertical stress of 18 kPa. This pressure cell is the only case in which the measured pressure is higher than the estimated *FLAC* value. The installation of this pressure cell was not different than at previous arrays, thus potential installation issues do not easily explain this difference.

# CONCLUSIONS

This paper presents field performance data from three geofoam embankments in the I-15 reconstruction in Salt Lake City, Utah and modeling results of these embankments using *FLAC*, a finite difference program. In general, *FLAC* produced reasonable estimates of the field measurements, both in terms of pressure distribution and vertical strain. We believe that numerical modeling of geofoam embankments provides valuable insight into the behavior and design of these complex, multi-layered systems

We found that the numerical model reasonably estimated the vertical and horizontal stress distributions that develop in geofoam embankments and the overlying materials. It reasonably predicted the magnitude of the measured stresses and their general trends throughout the embankment. However, some experience and care was required in interpreting the field measurements and relating them to the numerical results. For example, in some cases, installed pressure cells failed after a few months of operation. Also, cells placed above the geofoam, near the pavement surface, showed strong seasonal fluctuations due to differential expansion and contraction of the embankment and pavement systems.

The numerical modeling did not provide reliable estimates of the vertical stresses that developed in the base sand underlying the geofoam block. In almost all cases, the *FLAC* model over estimated the measured vertical stresses. We believe that some other phenomenon, not accounted for in the modeling approach and/or instrument installation,

affected the measurement and prediction of vertical stresses in the base sand. For example, it is possible that curvature in the geofoam block, or some other type of partial arch, has developed and does not allow for a uniform transfer of stress to the base sand.

We found that the vertical displacement and strain that develops upon initial loading in a geofoam embankment is relatively complex and is nonlinear. The relative vertical displacement of the geofoam embankment during construction loading was measured using magnet extensometers. In general, this type of instrumentation provided sufficient resolution to reasonably measure the vertical differential displacement as construction progressed. However, some magnet extensometer plates captured variations that were somewhat erratic. The variations were probably due to thermal expansion/contraction of the system and vertical displacement due to seating and gap closure at the block interfaces.

We propose that a bilinear elastic model can reasonably replicate the vertical strain behavior of geofoam embankments as verified by magnet extensometer measurements. In our bilinear model, we used an elastic modulus ranging from about 1.7 to 2.7 MPa to account for displacement occurring from block seating and gap closure between the surfaces of the untrimmed geofoam blocks for vertical stresses below 15 KPa. We found that an elastic modulus of 10 MPa can reasonably reproduce the measured compression of Type VIII geofoam at higher stress levels (i.e., above 15 kPa). At higher stress levels, it appears that elastic compression of the geofoam blocks dominates the state of stress.

The bilinear finite difference model has application in determining compression and contact stresses in settlement, slope stability and dynamic calculations. The

estimation of contact stresses is particularly important to sliding calculations that require determination of internal stability due to static and dynamic stresses. The results of this study and the *FLAC* models will be further used to determine the dynamic stability of geofoam embankments subject to near-field strong motion.

# REFERENCES

Bartlett, S., Negussey, D., Kimble, M., and Sheeley, M. (2000). "Use of Geofoam as Super-Lightweight Fill for I-15 Reconstruction." Transportation Research Board 79th Annual Meeting, Washington, D.C.

Bartlett, S.F., Farnsworth, C., Negussey, D., and Stuedlein, A.W. (2001). "Instrumentation and Long-Term Monitoring of Geofoam Embankments, I-15 Reconstruction Project, Salt Lake City, Utah." *Proceedings of the 3rd International EPS Geofoam Conference*, December 2001, Salt Lake City, Utah.

Bartlett, S.F. and Farnsworth, C.B. (2004). "Monitoring and Modeling of Innovative Foundation Treatment and Embankment Construction Used on the I-15 Reconstruction Project, Project Management Plan and Instrument Installation Report," UDOT Research Report No. UT-04.19, 202 p.

Benchmark Foam, Inc. (2003). "Physical Properties of EPS." April 4, 2004. <http://www.benchmarkfoam.com/benchmark/poly/properties.asp>

Elragi, A.F. (2000). "Selected Engineering Properties and Applications of EPS Geofoam." PhD Dissertation. State University of New York College of Environmental Science and Forestry, Syracuse, NY. 2000

Krahn, John. (2004). "Stress and Deformation Modeling with SIGMA/W: An Engineering Methodology." GEO-SLOPE International, Ltd. Calgary, Alberta, Canada.

Itasca Consulting Group, Inc. (2005). "*FLAC*: Fast Lagrangian Analysis of Continua: User's Guide." Minneapolis, Minnesota.

Itasca Consulting Group, Inc. (2005). "*FLAC*: Fast Lagrangian Analysis of Continua: Structural Elements, Version 5." Minneapolis, Minnesota.

Negussey, D., Stuedlin, A. W., Bartlett, S. F., and Farnsworth, C. "Performance of Geofoam Embankment at 100 South, I-15 Reconstruction Project, Salt Lake City, Utah." *EPS Geofoam 2001, 3rd International Conference*, December 2001, Salt Lake City, Utah, p. 22.

Negussey, D. and Studlein, A. (2003). "Geofoam Fill Performance Monitoring." Utah Department of Transportaion Research Division Report No. UT-03.17. August 2003.